JACS
JOURNAL OF THE AMERICAN CHEMICAL SOCIETY

ARTICLE

pubs.acs.org/JACS

$Gd_2@C_{79}N$: Isolation, Characterization, and Monoadduct Formation of a Very Stable Heterofullerene with a Magnetic Spin State of $S = 15/2$

Wujun Fu,[†] Jianyuan Zhang,[†] Tim Fuhrer,[†] Hunter Champion,[†] Ko Furukawa,[‡] Tatsuhisa Kato,[§] James E. Mahaney,[∥] Brian G. Burke,[⊥] Keith A. Williams,[⊥] Kenneth Walker,[#] Caitlyn Dixon,[†] Jiechao Ge,[†] Chunying Shu,[†] Kim Harich,[†] and Harry C. Dorn*[,†]

[†]Department of Chemistry, Virginia Polytechnic Institute and State University, Blacksburg, Virginia 24061, United States
[‡]Institute for Molecular Science, Okazaki, 444-8585, Japan
[§]Institute for the Promotion of Excellence in Higher Education, Kyoto University, Kyoto, 606-8501, Japan
[∥]Edward Via Virginia College of Osteopathic Medicine, Blacksburg, Virginia 24061, United States
[⊥]Department of Physics, Unviersity of Virginia, Charlottesville, Virginia, 22903, United States
[#]Luna Innovations, Inc. (nanoWorks division), 521 Bridge Street, Danville, Virginia 24541, United States

Supporting Information

ABSTRACT: The dimetallic endohedral heterofullerene (EHF), $Gd_2@C_{79}N$, was prepared and isolated in a relatively high yield when compared with the earlier reported heterofullerene, $Y_2@C_{79}N$. Computational (DFT), chemical reactivity, Raman, and electrochemical studies all suggest that the purified $Gd_2@C_{79}N$, with the heterofullerene cage, $(C_{79}N)^{5-}$ has comparable stability with other better known isoelectronic metallofullerene $(C_{80})^{6-}$ cage species (e.g., $Gd_3N@C_{80}$). These results describe an exceptionally stable paramagnetic molecule with low chemical reactivity with the unpaired electron spin density localized on the internal diatomic gadolinium cluster and not on the heterofullerene cage. EPR studies confirm that the spin state of $Gd_2@C_{79}N$ is characterized by a half-integer spin quantum number of $S = {}^{15}/_{2}$. The spin ($S = {}^{1}/_{2}$) on the N atom of the fullerene cage and two octet spins ($S = {}^{7}/_{2}$) of two encapsulated gadoliniums are coupled with each other in a ferromagnetic manner with a small zero-field splitting parameter D. Because the central line of $Gd_2@C_{79}N$ is due to the Kramer's doublet with a half-integer spin quantum number of $S = {}^{15}/_{2}$, this relatively sharp line is prominent and the anisotropic nature of the line is weak. Interestingly, in contrast with most Gd^{3+} ion environments, the central EPR line ($g = 1.978$) is observable even at room temperature in a toluene solution. Finally, we report the first EHF derivative, a diethyl bromomalonate monoadduct of $Gd_2@C_{79}N$, which was prepared and isolated via a modified Bingel–Hirsch reaction.

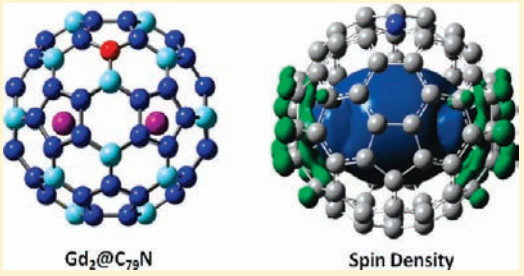

INTRODUCTION

Shortly after the discovery and macroscopic production of fullerenes, the idea of modifying the all-carbon sp^2 hybridized carbon surface of fullerenes has been an intriguing area of fullerene research. For example, fullerenes with icosahedral symmetry cages (e.g., C_{60} and C_{80}) that have single atom replacement (doping) with a trivalent heteroatom (N or B) leads to nearly spheroidal heterofullerene radicals which could have numerous applications.[1−3] Wudl and co-workers first reported the preparation of the unstable aza(60) fullerene ($C_{59}N$), which is easily dimerized as the corresponding dimer species $(C_{59}N)_2$.[4]

For the larger C_{80} cage system, it is well recognized that trimetallic nitride template (TNT) endohedral metallofullerenes (EMFs), such as, $M_3N@C_{80}$ and $M_2@C_{80}$ (M = metals) have highly stabilized icosahedral carbon $(C_{80})^{6-}$ cages. The stability of the aza(C_{80}) fullerene ($C_{79}N$) cage was first recognized by Akasaka and co-workers who reported evidence for $(La_2@C_{79}N)^{+}$ by mass spectrometry.[5] Other workers have reported computational studies supporting the stability of related heterofullerenes $Sc_3N@C_{79}N$, $Sc_3N@C_{79}B$, and $Sc_3N@C_{78}BN$.[6] More recently, our laboratory has reported the isolation and characterization of the paramagnetic dimetallic endohedral heterofullerenes (EHFs), $Y_2@C_{79}N$ and $Tb_2@C_{79}N$.[7] The EPR studies of $Y_2@C_{79}N$ indicate that the unpaired spin density is mainly localized between the two equivalent yttrium ions and not on the heterofullerene cage.[7] Also, the trimetallic nitride cluster $(La_3N)^{6+}$ has been reported by Stevenson and co-workers in the same $C_{79}N$ cage, namely, $La_3N@C_{79}N$.[8] Surprisingly, it was found that the large La_3N cluster was preferentially encapsulated in a $C_{79}N$ cage, but not in a C_{80} cage (e.g., $La_2@C_{80}$).[8] However, most studies of EHFs are based on computational studies because experimental isolation and detailed characterization is extremely difficult due to the

Received: July 19, 2010
Published: May 06, 2011

dx.doi.org/10.1021/ja202011u | J. Am. Chem. Soc. 2011, 133, 9741–9750

small amount of sample usually available and the difficulty in the separation and characterization of EHFs.

Gadolinium-based endohedral metallofullerenes (e.g., $Gd@C_{82}$, $Gd_3N@C_{80}$) represent an important class of new nanomaterials since it is well recognized that these have important magnetic properties and are actively being explored as next-generation magnetic resonance imaging (MRI) contrast agents.[9−16] Herein, we report the preparation, purification, and spectroscopic studies of the first gadolinium-based EHF, namely, $Gd_2@C_{79}N$. All theoretical and experimental studies confirm that this unique EHF displays an unusually high stability with an impressive yield compared with other EHFs reported to date.[7,8] The magnetic properties for this paramagnetic molecule are also very interesting since the seven unpaired f electrons for each Gd^{3+} ion within the cage can interact with an additional unpaired electron formally provided by the nitrogen atom on the heterofullerene $C_{79}N$ cage. Additionally, the first successful functionalized gadolinium-based EHF is also reported and isolated.

EXPERIMENTAL AND COMPUTATIONAL METHODS

Preparation and Separation of $Gd_2@C_{79}N$. The preparation of $Gd_2@C_{79}N$ was accomplished utilizing a Krätschmer-Huffman (K−H) generator as described previously.[7,17] Specifically, soot containing $Gd_2@C_{79}N$ and other fullerenes and endofullerenes were synthesized in a K−H generator by vaporizing composite graphite rods containing a mixture of gadolinium oxide, Gd_2O_3, graphite powder, and metallic Cu with a weight ratio of 2.0:1.0:2.1 in a dynamic flow of He and N_2 (flow rate ratio of N_2/He = 3:100). The resulting soot was then extracted with refluxing toluene in a Soxhlet extractor and the soluble extract was applied to a cyclopentadiene-functionalized Merrifield peptide resin (CPDE-MPR) column.[18] As previously reported, most of the empty cage fullerenes and more reactive classical endofullerenes are retained on the CPDE-MPR column. There are seven distinct fractions obtained utilizing a pentabromobenzyl (PBB) HPLC column in similar fashion to results reported previously for other metal ions as shown in Figure 1. To estimate the overall yield, the relative yield ratio of $Gd_2@C_{79}N/C_{60}$ is ∼0.05−0.1% using the current preparation and separation protocol; that is, for every gram of C_{60} formed we can isolate 0.5−1 mg of $Gd_2@C_{79}N$. Although this yield is relatively low, it is still ∼10 times greater than achieved for $Y_2@C_{79}N$ (see Figure 1).

Synthesis of the Diethyl Bromomalonate Monoadduct of $Gd_2@C_{79}N$. Approximately 100 μg of $Gd_2@C_{79}N$ was dissolved in 2 mL toluene, and ∼20 equivalent of diethyl bromomalonate (Aldrich Chemical Co.) and ∼10 equivalents of 1,8-Diazabicycloundec-7-ene (DBU, Aldrich Chemical Co.) was added for the synthetic preparation and reactivity comparison study, respectively. Finally, a drop of DMF was added with a syringe as a catalyst. The reaction mixtures were degassed and subsequently stirred at room temperature for 40 and 60 min, respectively. The product was isolated by HPLC.

Characterization. Mass spectrometry was performed on a Kratos Analytical Kompact SEQ LD-TOF mass spectrometer. Cyclic voltammetry (CV) was conducted using a CH Instruments 600A potentiostat (Austin, TX) with a single-compartment electrochemical cell. A 2.0 mm glassy carbon working electrode, a platinum wire auxiliary electrode and a silver wire pseudo-reference electrode were used; ferrocene was added as an internal standard. The x-band EPR spectrum of $Gd_2@C_{79}N$ at 4K was obtained by using a Bruker E500 spectrometer. The w-band EPR spectrum of $Gd_2@C_{79}N$ at 30K was obtained by using a Bruker E680 spectrometer. Other EPR spectra were recorded with a Bruker D200 ER IBM-Bruker spectrometer.

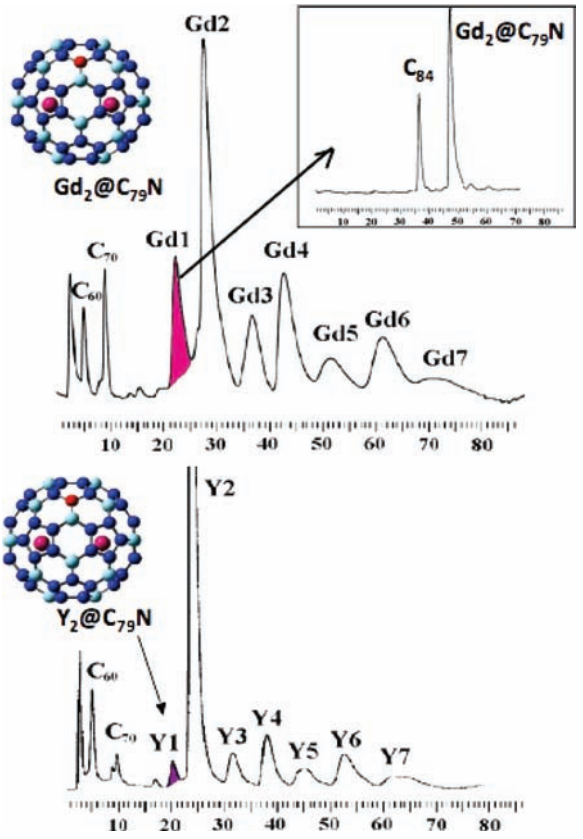

Figure 1. HPLC Chromatography of soot extracts containing Gd1 (top) and Y1 fractions (bottom) utilizing a PBB column; λ = 390 nm; flow rate 2.0 mL/min; toluene as eluent; 25 °C; upper right insert HPLC chromatographic $Gd_2@C_{79}N$ and $Y_2@C_{79}N$ separation with a PYE column; λ = 390 nm; flow rate 2.0 mL/min; toluene as eluent; 25 °C.

Computational Study. Density functional theory (DFT) computations were performed using the spin-unrestricted B3LYP functional as provided in the Gaussian 03 program package.[19] All of the molecules were geometry optimized at the UB3LYP level with a 6-31G* basis set for carbon and nitrogen atoms and the CEP-121G basis set for gadolinium atoms. DFT-optimized energy values were obtained starting from the X-ray crystallographic structures of the corresponding $Tb_2@C_{79}N$.[7] The DFT computations employed the PBE0 functional[20] as described in the Gaussian 09[19] program package and were utilized for $Gd_2@C_{79}N$ in an effort to properly treat the unpaired electrons on the gadolinium atoms, while the B3LYP functional set[21−23] was used for the empty cage calculations. The 6-31G basis set[24] was used for all carbon and nitrogen atoms in all computations.

RESULTS AND DISCUSSIONS

Preparation and Separation of $Gd_2@C_{79}N$. A sample of $Gd_2@C_{79}N$ was synthesized by utilizing a Krätschmer-Huffman (K−H) generator by vaporizing graphite rods containing a mixture of Gd_2O_3 and graphite powder and Cu as a catalyst. The toluene extract from the raw soot was applied to a CPDE-MPR. The eluent was further separated by two-stage HPLC.[17] The first stage was carried out on a 5PBB column and there are seven distinct fractions obtained utilizing 5PBB HPLC column in similar fashion to results reported previously for other metal clusters as shown in Figure 1.[17] The first fraction Gd1 obtained

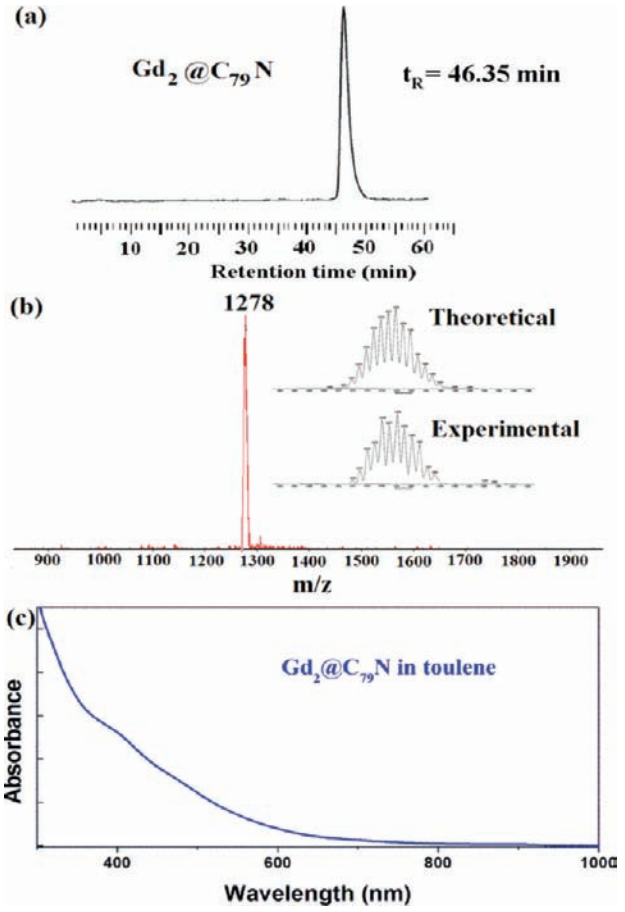

Figure 2. (a) HPLC Chromatography of $Gd_2@C_{79}N$ (a 10 × 250 mm 5PYE column; λ = 390 nm; flow rate 2.0 mL/min; toluene as eluent; 25 °C); (b) positive ionization LD-TOF mass spectra of $Gd_2@C_{79}N$, Inset: theoretical and experimental isotopic distribution of $Gd_2@C_{79}N$ comparison; (C) UV−vis spectrum of $Gd_2@C_{79}N$ in toluene.

from the PBB column contains C_{84} and $Gd_2@C_{79}N$, which was further purified by a 5PYE column as illustrated in the top inset of Figure 1. An unusual feature of the preparation and separation process is the significantly higher yield of $Gd_2@C_{79}N$ in comparison with the previously reported $Y_2@C_{79}N$ as illustrated in Figure 1. The higher yield at this stage in the separation is either due to a higher inherent yield in the K−H generator and/or lower chemical Diels−Alder reactivity of $Gd_2@C_{79}N$ in comparison with $Y_2@C_{79}N$ on the CPDE-MPR column, and this point is discussed *vide infra.*

The purity of $Gd_2@C_{79}N$ was confirmed by laser-desorption time-of-flight (LD-TOF) mass spectrometry. The HPLC chromatogram, LD-TOF mass spectrum, and the UV−vis absorption spectrum of the purified $Gd_2@C_{79}N$ is shown in Figure 2. When compared with $Y_2@C_{79}N$ and $Tb_2@C_{79}N$, the similarity of UV−vis spectra and chromatographic retention behavior of $Gd_2@C_{79}N$ indicate a close correspondence of these cage structures (See Supporting Information and Figure 3).[7]

Comparative Diels−Alder Reactivity Study of $Gd_2@C_{79}N$ and $Y_2@C_{79}N$. Although the enhanced stability of the icosahedral $(C_{80})^{6-}$ cage is well documented, the stability of the isoelectronic $(C_{79}N)^{5-}$ cage is not as well recognized. As noted above, a surprising feature of $Gd_2@C_{79}N$ was the significantly higher yield of $Gd_2@C_{79}N$ obtained in the separation process in comparison with $Y_2@C_{79}N$ (Figure 1). This enhanced yield is either due to a higher inherent yield in the K−H electric-arc generator process and/or lower chemical Diels−Alder reactivity of $Gd_2@C_{79}N$ in comparison with $Y_2@C_{79}N$ during the chemical CPDE-MPR separation process. To test between these alternatives, we prepared a two-component mixture (in toluene) containing nearly equal quantities of pure $Gd_2@C_{79}N$ and $Y_2@C_{79}N$ samples; the overall process is outlined in Figure 3. As expected, these two heterofullerenes have very similar chromatographic retention times and are only slightly resolved on a PYE column. A two-component mixture of $Gd_2@C_{79}N$ and $Y_2@C_{79}N$ was applied a second time to the CPDE-MPR column as summarized in Figure 3. Greater than 70% of the mixture was recovered from the (CPDE-MPR) column and the resulting mixture exhibits a slight enhancement (∼5−10%) in the concentration of the $Gd_2@C_{79}N$ species. This preferential reaction of the $Y_2@C_{79}N$ species was confirmed by heating the recovered cyclopentadiene-functionalized Merrifield peptide resin under reflux conditions in toluene for 12 h. The resulting toluene solution was concentrated and mass spectral analysis on the recovered sample indicates a preponderance of the $Y_2@C_{79}N$ species (Figure 3c). These results confirm very low chemical reactivity of both $Gd_2@C_{79}N$ and $Y_2@C_{79}N$ toward the cyclopentadiene moiety on the Merrifield peptide supported column.[18] Thus, we observe a slightly enhanced Diels−Alder chemical reactivity of the $Y_2@C_{79}N$ species in comparison with $Gd_2@C_{79}N$ toward the supported cyclopentadiene moiety. These results are consistent with an enhanced yield of the $Gd_2@C_{79}N$ species in the K−H electric-arc process, and a slightly lower Diels−Alder chemical reactivity relative to $Y_2@C_{79}N$. These results suggest that an optimum size of the $(M_2)^{5+}$ cluster is necessary for optimizing metal−carbon cage bonding in the $(C_{79}N)^{5-}$ cage. This is also consistent with the optimized formation of the $(La_3N)^{5+}$ cluster in the $(C_{79}N)^{5-}$ cage ($La_3N@C_{79}N$), but not in the isoelectronic $(C_{80})^{6-}$cage.[8]

Computational Studies of the Heterofullerenes $[C_{79}N]^{5-}$ and $Gd_2@C_{79}N$. Because of the recent experimental success in preparing stable heterofullerenes with $(C_{79}N)^{5-}$ cages with different endohedral clusters $(M_2)^{5+}$ and $(La_3N)^{5+}$ [7,8], we have explored the stability of the heterofullerene cage alone and with two Gd^{3+} encapsulated ions by density functional theory (DFT) computations using the spin-unrestricted B3LYP functional in the Gaussian 03 program.[19] For the I_h-C_{80} cage there are two types of carbon atoms: 60 carbon atoms reside at pentagon sites at a 665 junction, while the remaining 20 carbons are not at pentagon sites but reside at the junctions of three hexagons (a 666 junction). Our studies have confirmed that the nitrogen atom in the I_h-C_{80} cage is significantly more stable at the 665 junction (pentagon) position than the 666 junction and this cage with a $(Gd_2)^{5+}$ cluster yields $Gd_2@C_{79}N$.[6] Thus, encapsulation of the dimetallic cluster into a C_{79} cage with a N at the 665 junction is favored.

As shown in Figure 4, the heterofullerene $(C_{79}N)^{5-}$ and isoelectronic I_h-$(C_{80})^{6-}$ cage both have relatively large HOMO−LUMO gaps of 2.67 and 3.16 eV, respectively. These values are similar to the HOMO−LUMO gaps for other well-known stable $M_3N@I_h$-C_{80} molecules.[25−28] It is also significant that the HOMO level and total energy of the heterofullerene cage $(C_{79}N)^{5-}$ is even lower than isoelectronic $(C_{80})^{6-}$. However, when an extra electron is added (Figure 4c) to the cage surface, the LUMO−HOMO gap of the resulting $(C_{79}N)^{6-}$ is relatively small (1.47 eV) and is destabilized relative to $(C_{79}N)^{5-}$. This

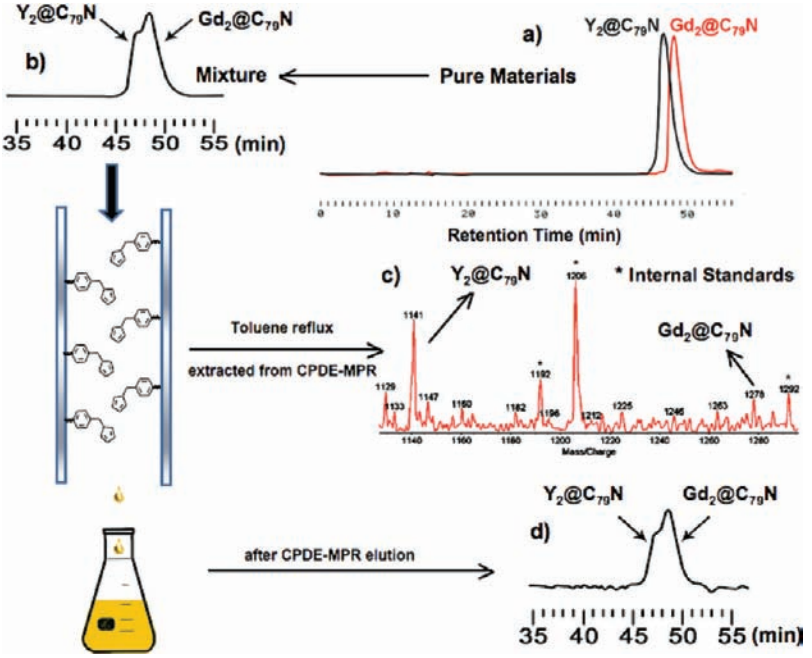

Figure 3. (a) HPLC of pure $Gd_2@C_{79}N$ and $Y_2@C_{79}N$ samples (a) and the mixture (b) before and after separation and reaction on a CPDE-MPR column (a 10 × 250 mm 5PYE column; λ = 390 nm; flow rate 2.0 mL/min; toluene as eluent; 25 °C); (c) Negative ion ionization LD-TOF mass spectra of recovered $Gd_2@C_{79}N$ and $Y_2@C_{79}N$ mixture from CPDE-MPR column with internal standard $C_{23}H_{15}O_6N_3P_3F_{36}$.[18] (d) HPLC of recovered $Gd_2@C_{79}N$ and $Y_2@C_{79}N$ mixture.

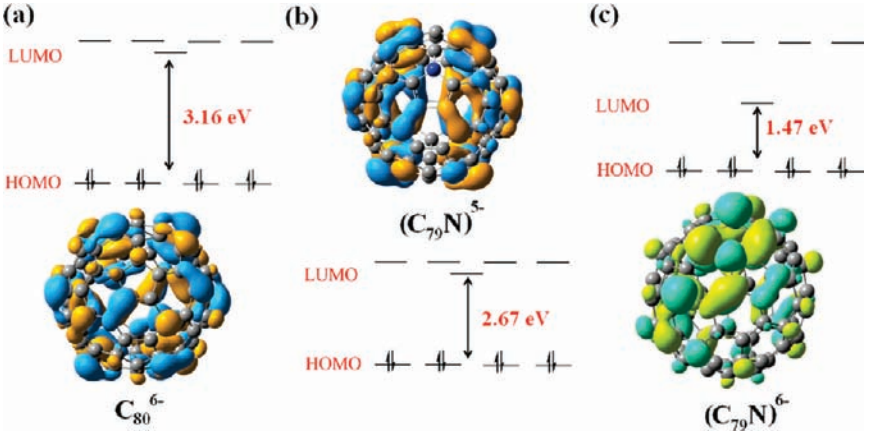

Figure 4. DFT HOMO−LUMO levels of $(C_{80})^{6-}$, $(C_{79}N)^{5-}$, $(C_{79}N)^{6-}$ cages.

result is consistent with the notion that both $(M_2)^{5+}$ and $(La_3N)^{5+}$ endohedral clusters would be suitable for stabilization of a heterofullerene $(C_{79}N)^{5-}$ cage and the internal cluster can accept the unpaired electron formally from the N atom of the fullerene cage.

Extension of the DFT computational approach to $Gd_2@C_{79}N$ (PBEO functional) and the CEP-121G basis set for gadolinium atoms provides energy levels that are comparable with the previously reported $Y_2@C_{79}N$ system (Figure 5).[7] The computed HOMO−LUMO gap for $Gd_2@C_{79}N$ (2.74 eV) is slightly larger than the previously computed HOMO−LUMO gap for $Y_2@C_{79}N$ (2.39 eV).[7] Careful examination of each HOMO level indicates no significant Gd−Gd bonding overlap until the HOMO-7 to HOMO-22 levels. We assign the former HOMO-7 level as the highest of the fifteen singly occupied molecular orbitals (SOMO) on $Gd_2@C_{79}N$. The HOMO-7 SOMO orbital can be described in terms of a natural bonding order (NBO) as a $Gd(s^1p^{0.95}d^{0.11}f^{0.06})$−$Gd(s^1p^{0.95}d^{0.11}f^{0.06})$ bond. In analogous fashion with $Y_2@C_{79}N$, $Gd_2@C_{79}N$ represents another example of spin-polarized orbitals that occur at energy levels below the HOMO.[7] The large degree of s character on the Gd_2 cluster as well as the α spin densities illustrated in Figure 6 for both $Gd_2@C_{79}N$ and $Y_2@C_{79}N$ clearly indicate unpaired electron spin density localized between the two Gd atoms and not delocalized on the heterofullerene cage. Although we previously reported the spin density for $Y_2@C_{79}N$, a significant difference is the higher degree of p and f orbital hybridization in the $Gd_2@C_{79}N$ case.[7] The significant s-orbital Fermi contact is also an important feature in understanding the EPR spectra *vide infra*. The computed Gd−Gd bond length for

dx.doi.org/10.1021/ja202011u |*J. Am. Chem. Soc.* 2011, 133, 9741–9750

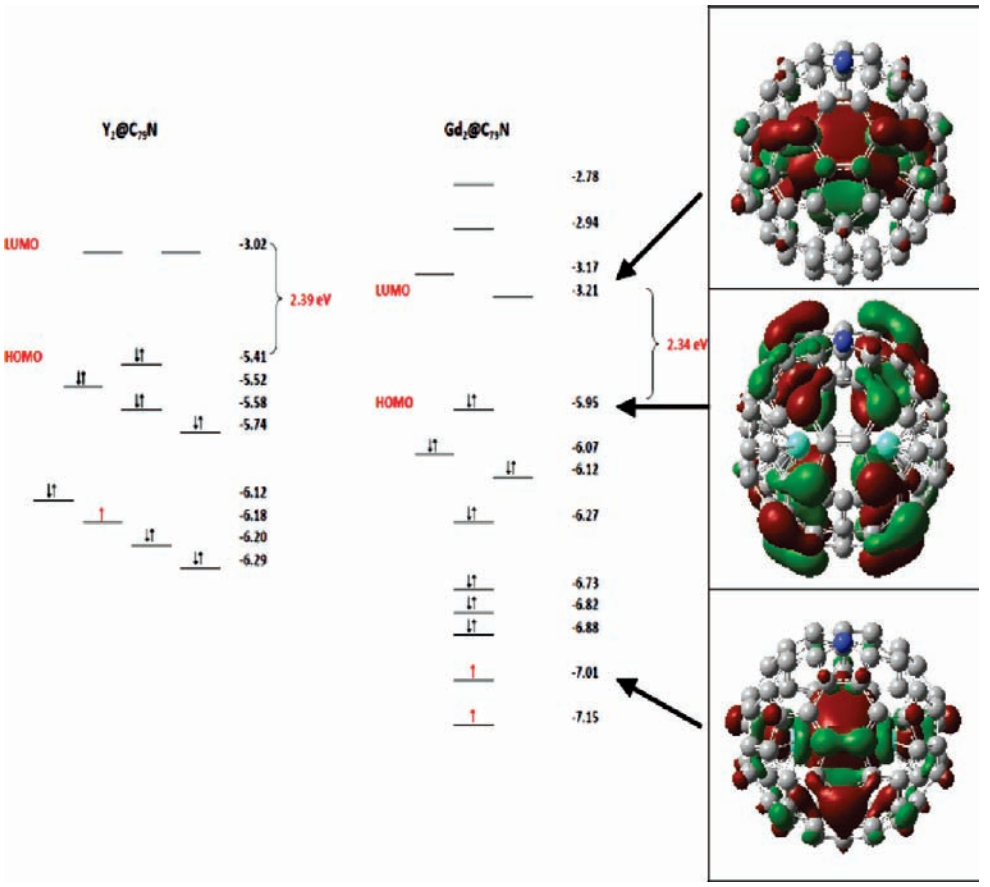

Figure 5. DFT MO energy level diagrams for optimized $Y_2@C_{79}N$ (from ref 7) and $Gd_2@C_{79}N$ (LUMO, HOMO and HOMO-7 orbitals shown).

$Gd_2@C_{79}N$ is 3.808 Å. This is another example of a long M−M bond, but is close to the Tb−Tb distance of the X-ray crystallographic value for $Tb_2@C_{79}N$ (3.902 Å) and the previously computed Y−Y distance in $Y_2@C_{79}N$ (3.994 Å).[7] The electrostatic metal ion repulsion within these M_2^{5+} units and fullerene cage restrictions are clearly important factors in determining the M−M bond distances.

Electrochemical Studies of $Gd_2@C_{79}N$. Electrochemical studies provide an excellent approach to further understand the redox chemistry of metallofullerenes and the unusual electronic and magnetic properties of $Gd_2@C_{79}N$. Specifically, cyclic voltammetry electrochemical data for $Gd_2@C_{79}N$ is directly compared with $Gd_3N@C_{80}$ under the same conditions (Figure 7). In addition, this data is compared with other related endohedral metallofullerenes and summarized in Table 1. The electrochemical response for $Gd_2@C_{79}N$ exhibits an electrochemically reversible oxidation accompanied by two prominent reduction potentials; the first reduction peak is reversible with a half-wave potential ($E_{1/2}^{red1}$ = −0.96 V) and the second reduction is irreversible at −1.98 V. The order of the first reduction potentials for $La_2@C_{80}$, $Gd_2@C_{79}N$, and $Gd_3N@C_{80}$ are $E_{1/2}^{red1}$ = −0.31 V, $E_{1/2}^{red1}$ = −0.96 V, and $E_{1/2}^{red1}$ = −1.44 V, respectively. It has previously been reported that the low first reduction potential of $La_2@C_{80}$ is associated with a lower LUMO level in comparison with other trimetallic nitride endohedral metallofullerenes (e.g., $Gd_3N@C_{80}$ and $Y_3N@C_{80}$)[40] whereas the first reversible reduction of $Gd_2@C_{79}N$ is significantly different and can be assigned to the low-lying SOMO *vide supra*.

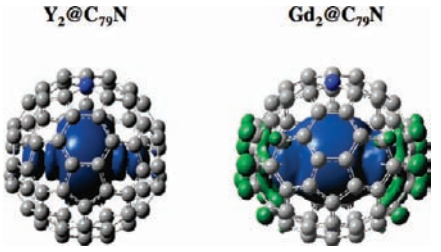

Figure 6. Unpaired spin density (α) distribution for $Y_2@C_{79}N$ and $Gd_2@C_{79}N$.

The oxidation of $[Gd_2@C_{79}N]^-/[Gd_2@C_{79}N]^0$ is not as kinetically favored as the forward reversible reduction reaction as shown by scan rate dependence (Supporting Information). One explanation of this is a possible structural rearrangement when the SOMO is filled due to the change in bond order of the Gd−Gd complex. The question of the reversibility of the first oxidation and reduction steps for $Gd_2@C_{79}N$ was explored in greater detail with additional cyclic voltammetry experiments as well as independent samples (see Supporting Information).

EPR Studies of $Gd_2@C_{79}N$. For most lanthanide ions, it is well recognized that the corresponding EPR signals are not readily observed at room temperature because of relatively short electron spin−lattice relaxation times ($T_{1e} < 10^{-8}-10^{-9}$ s) with large zero-field splitting parameters (D) and corresponding broad EPR line widths for these f-orbital ions.[29] In contrast, the X-band EPR spectrum (Figure 8) for a dilute solution of

dx.doi.org/10.1021/ja202011u |*J. Am. Chem. Soc.* 2011, 133, 9741–9750

$Gd_2@C_{79}N$ in toluene exhibits a broadened, but observable, symmetric spectral line with a g-factor 1.978 similar to $Y_2@C_{79}N$ (g = 1.9740) at 298 K. A solid sample of $Gd_2@C_{79}N$ at room temperature exhibits increased broadening due to increased Heisenberg exchange. This effect was confirmed by a solid-state dilution experiment where the $Gd_2@C_{79}N$ sample was mixed with an empty cage fullerene C_{60} (ratio of C_{60}: $Gd_2@C_{79}N$ ~9:1; see Supporting Information). There is a small sharp peak with the observed g-factor (g_0 = 2.001), which has been previously reported as defect sites in C_{60} cages[30] (see Supporting Information). The ambient temperature EPR spectrum of the solution and mixed solid sample suggests considerable motional averaging motion of the $Gd_2@C_{79}N$ molecule and/or Gd−Gd cluster motional averaging in the C_{60} solid matrix without an observable nuclear hyperfine interaction.

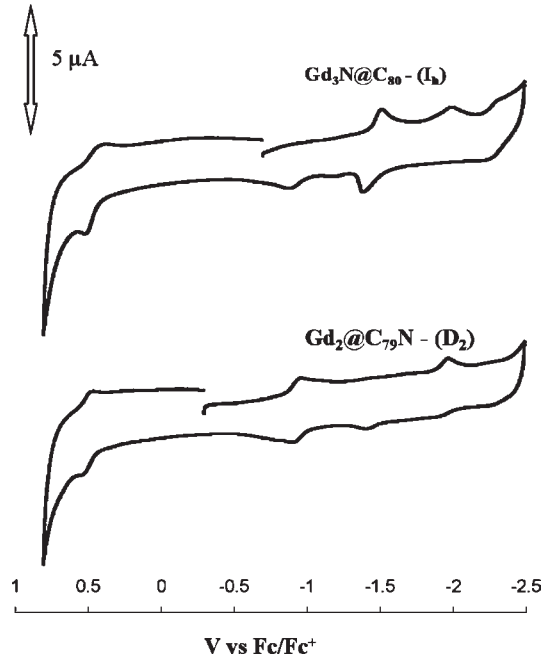

Figure 7. Cyclic voltammogram of (a) $Gd_3N@C_{80}$ and (b) $Gd_2@C_{79}N$ in *o*-dichlorobenzene, 0.1 M $TBABF_4$, 100 mV/s scan rate.

Table 1. Redox Potentials of $Gd_2@C_{79}N$ and Related EMFs

	E_{pc}^{red1}	E_{pc}^{red2}	$E_{1/2}^{ox1}$	ΔE
$La_2@C_{80}$[37][a]	−0.31	−1.72	0.56	0.87
$Gd_2@C_{79}N$	−0.96	−1.98	0.51	1.47
$Gd_3N@(I_h)$-C_{80}	−1.44	−1.86	0.58	2.02
$Y_3N@(I_h)$-C_{80}	−1.41	−1.83	0.64	2.05

[a])Reversible electrochemical redox potentials. Values vs ferrocene.

In contrast, low temperature X-band and W-band EPR spectra of $Gd_2@C_{79}N$ were also obtained, as shown in Figure 9. Both spectra are featured by the fine structure of a high spin state. The w-band measurement gives a more simplified spectrum, which is almost symmetric around the intense central line, as shown in Figure 9b. Seven peaks on both sides of the central line at equidistant intervals can be recognized (inset of the Figure 9b), and a total of 15 peaks can be counted. The 15 peaks suggest the spin quantum number of $^{15}/_2$ for the spin state of $Gd_2@C_{79}N$. As previously reported,[31] the ground spin state of $Gd@C_{82}$−I is characterized by an integer spin quantum number of S = 3. The spin ($S = {}^1/_2$) on the π orbital of the fullerene cage is coupled with the octet spin ($S = {}^7/_2$) of the encapsulated gadolinium in an antiferromagnetic manner with the exchange coupling constant of $J = -1.8$ cm^{-1}. In the case of $Gd_2@C_{79}N$, however, the spin state is characterized by a half-integer spin quantum number of $S = {}^{15}/_2$. The spin ($S = {}^1/_2$) on the N atom of the fullerene cage and two octet spins ($S = {}^7/_2$) of two encapsulated gadoliniums are coupled with each other in a ferromagnetic manner. The difference of the electronic state of $Gd_2@C_{79}N$ also reflects its small zero-field splitting parameter D. The value of D is estimated about 70 mT for $Gd_2@C_{79}N$, which is much smaller than the D = 420 mT of $Gd@C_{82}$−I.

Because the central line of $Gd_2@C_{79}N$ is due to the Kramer's doublet in the state with a half-integer spin quantum number of $S = {}^{15}/_2$, the sharpness of the line is prominent and the anisotropic nature of the line is weak. As a result the sharp

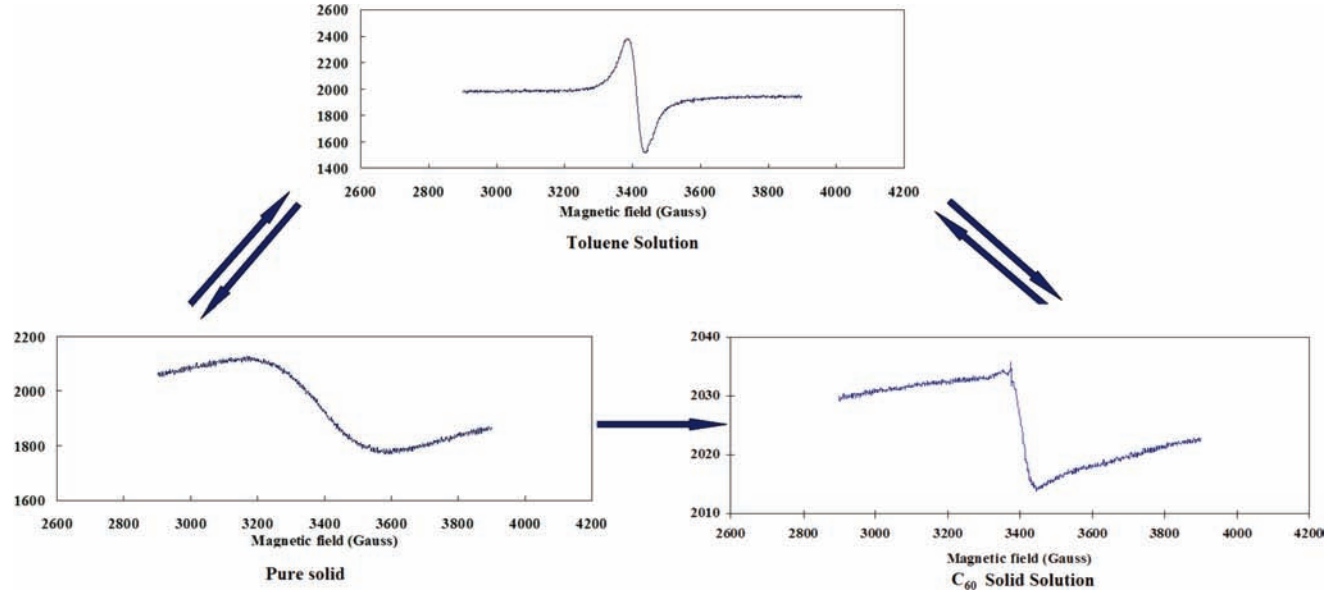

Figure 8. EPR spectra of $Gd_2@C_{79}N$ samples at 298 K in toluene solution, as a solid, and as a solid solution with C_{60}.

dx.doi.org/10.1021/ja202011u |*J. Am. Chem. Soc.* 2011, 133, 9741–9750

central line is observable even at room temperature in solution *vide supra*. The other surprising feature of $Gd_2@C_{79}N$ is a long spin relaxation time, which enables the detection of electron spin echo (ESE) signal by a pulsed EPR spectrometer even at 20 K. It is rather exceptional that a pulsed EPR observation is applicable to the high spin system of $S = {}^{15}/_{2}$ (see Supporting Information).

Raman Spectroscopy. As described above, $Gd_2@C_{79}N$ has a similar structure to $Gd_3N@C_{80}$[32] and $Sc_3N@C_{80}$,[33] which have previously been studied by Raman spectroscopy, except that a nitrogen atom, donating a free electron, has replaced one carbon atom in the cage and the endohedral cluster is a $(Gd_2)^{5+}$ dimer. The full Raman spectrum of $Gd_2@C_{79}N$ is shown in Figure 10 and can be divided into four parts: low intensity modes above 1700 cm^{-1}, tangential $C_{79}N$ modes are found between 1000 and 1700 cm^{-1}, radial $C_{79}N$ modes between 200 and 1000 cm^{-1}, and a fourth group from 200 cm^{-1} and below which has a counterpart only in the spectra of endohedral fullerenes which exhibit low energetic Gd-fullerene cage, intermolecular, and center-of-mass (COM) modes. Low-energy Raman modes of endohedral fullerenes ($Gd_3N@C_{80}$ and $Sc_3N@C_{80}$) have been observed previously, confirming the coupling between the core and the cage by hindered rotation modes.[29,30] We observe similar hindered rotation modes for $Gd_2@C_{79}N$ at 156.1 and 170.4 cm^{-1}.

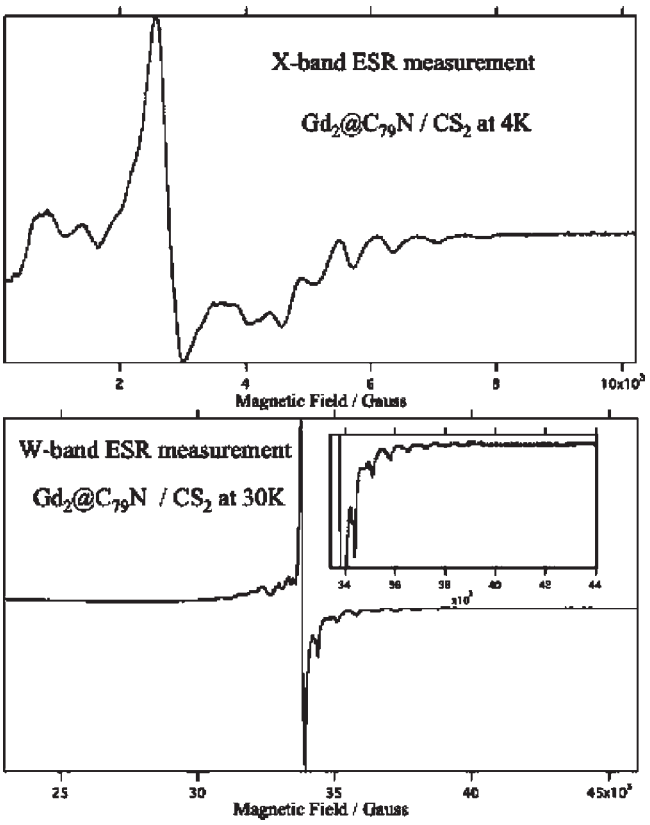

Figure 9. (a) X-band EPR spectrum of $Gd_2@C_{79}N$ sample at 4 K in CS_2; (b) W-band EPR spectrum of $Gd_2@C_{79}N$ sample at 30 K; vertical expansion, horizontal axis, 34−44 × 10^2 gauss.

The vibrational modes of $Gd_2@C_{79}N$ and $Gd_3N@C_{80}$ were calculated by hybrid DFT (B3LYP) and UFF in the Gaussian 03 package[34] and compared with the experimental data. We identify tangential and radial $C_{79}N$ cage modes, which are similar to the C_{80} cage modes. A comparison of the $Gd_2@C_{79}N$ and $Gd_3N@C_{80}$ experimental data is shown in Figure 11. In particular, we identify the $H_g(1)$ squashing mode at 226 cm^{-1} for $Gd_2@C_{79}N$ and at 234 cm^{-1} for $Gd_3N@C_{80}$.

Additionally, upon further investigation of low-energy Raman modes (Figure 12) and comparison with the theoretical model, $Gd_2@C_{79}N$ hindered rotation and COM modes are observed below 200 cm^{-1}. A Gd−Gd stretching mode is observed at 52.4 cm^{-1} and confirmed by simulations. The Gd−cage mode at 156.1 cm^{-1} has a very narrow peak, which is attributed to a Gd−Gd stretch mode interacting with the $C_{79}N$ cage and the Gd_2 confinement in the smaller $C_{79}N$ cage, when compared to similar molecules with larger cages, such as $Gd_2@C_{90}$.[35]

Bingel−Hirsch $Gd_2@C_{79}N$ Diethyl Bromomalonate Monoadduct. We have previously described the exceptional chemical stability of $Gd_2@C_{79}N$ and corresponding low Diels−Alder reactivity (Figure 3) and relatively large HOMO−LUMO gap (Figures 4 and 5) from the computational studies. Although purified sample quanities were limited to ∼1 mg, other unsuccessful chemical reactions were explored and summarized (Figure 13). For example, in similar fashion with $Y_2@C_{79}N$, we found no evidence of dimerization of $Gd_2@C_{79}N$, which

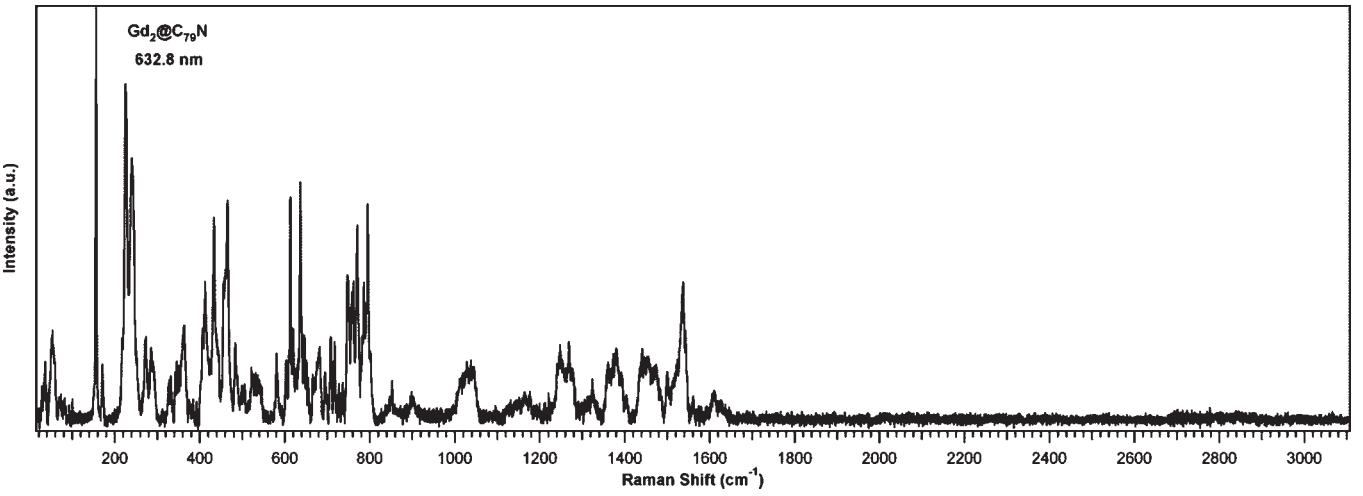

Figure 10. Analysis of full Raman spectra for $Gd_2@C_{79}N$ taken at 90 K. Tangential and radial $C_{79}N$ modes are observed, as well as hindered rotation and COM modes.

dx.doi.org/10.1021/ja202011u |*J. Am. Chem. Soc.* 2011, 133, 9741–9750

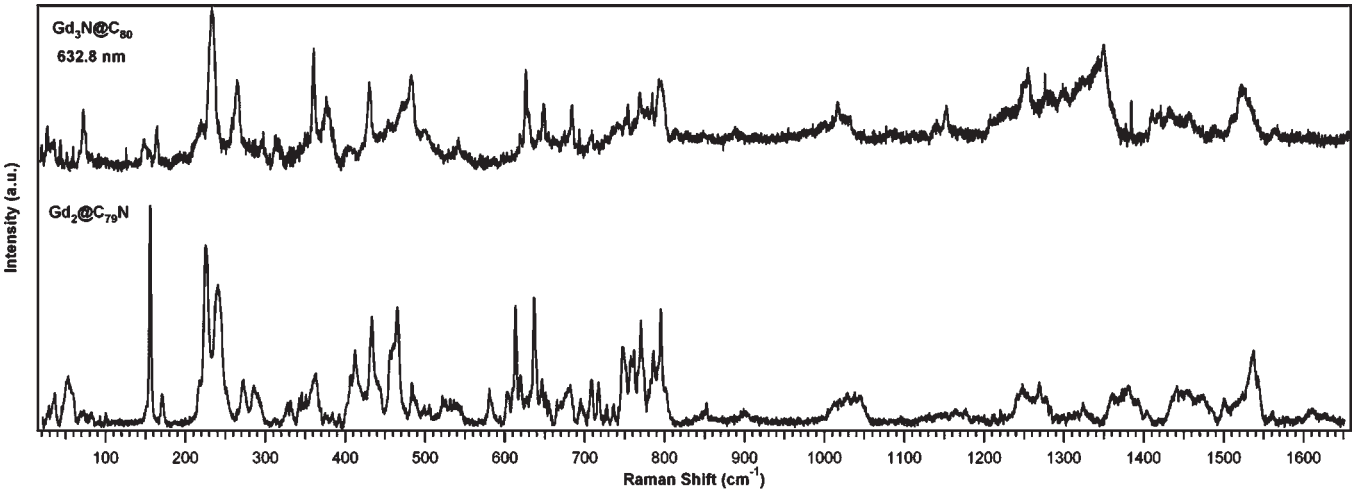

Figure 11. Comparison of $Gd_2@C_{79}N$ and $Gd_3N@C_{80}$ Raman spectra taken at 90 K. The $C_{79}N$ and C_{80} cage modes are comparable, and both samples exhibit hindered rotation modes below 200 cm^{-1}.

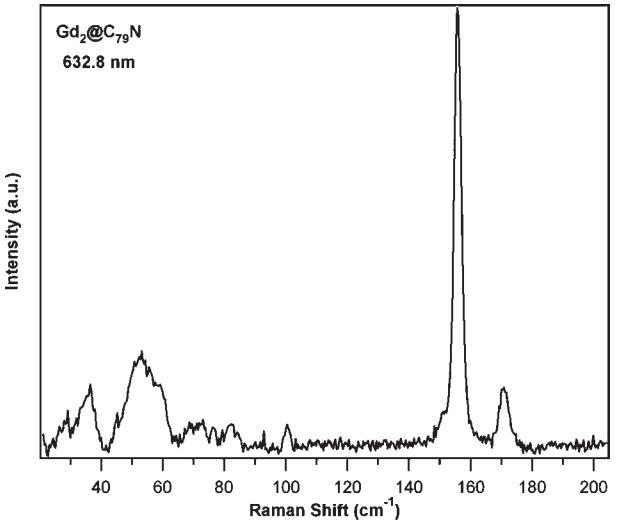

Figure 12. Analysis of low-energy Raman spectra of $Gd_2@C_{79}N$ taken at 90 K, indicating hindered rotation due to the coupling of the core complex to the cage. There is a strong Gd−Gd stretching mode at 52.4 cm^{-1} and a narrow Gd−cage stretching mode at 156.1 cm^{-1}.

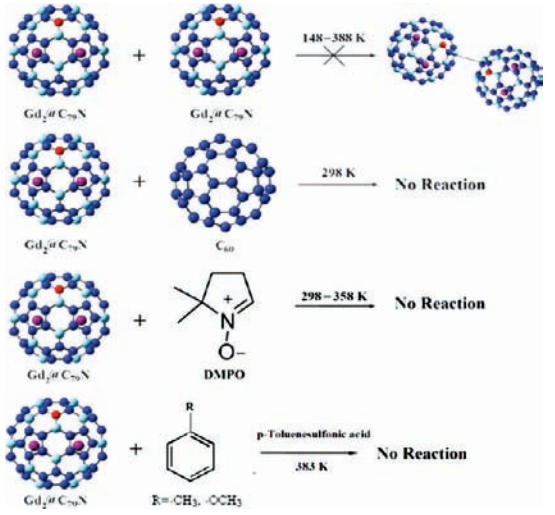

Figure 13. Chemical reactivity summary of $Gd_2@C_{79}N$.

readily occurs with $C_{59}N$.[1] In an attempt to explore known heterofullerene reactions of $C_{59}N$, the arylation in the presence of p-toluenesulfonic acid with toluene of anisole,[36] does not lead to any product in observable quantities. Alternatively, we attempted a chemical reaction of 5,5-dimethyl-1-pyrroline-1-oxide (DMPO), a well-known spin trap[37] with $Gd_2@C_{79}N$ in toluene, but the resulting EPR spectrum provides no evidence of a chemical reaction between DMPO and $Gd_2@C_{79}N$. This low chemical reactivity of $Gd_2@C_{79}N$ is consistent with an exceptionally stable molecule with the unpaired electron spin density mainly localized between the Gd metal atoms and is not easily localized on the heterofullerene cage surface.

In spite of this low chemical reactivity, the first successful functionalization of $Gd_2@C_{79}N$ was achieved via a Bingel-Hirsch reaction by cyclopropanation with diethyl bromomalonate, but only in the presence of DMF (Figure 13).[38] To directly compare the reactivity of $Gd_3N@C_{80}$, $Sc_3N@C_{80}$ and $Gd_2@C_{79}N$, we prepared toluene solutions of these three purified metallofullerenes respectively in nearly equal molarities and performed Bingel−Hirsch reactions under the same conditions. Approximately 20 equiv of diethyl bromomalonate, 10 equiv of 1,8-diazabicyclo[5.4.0]undec-7-ene (DBU) and 1 drop of DMF were added to the solutions under argon at room temperature. All three reaction mixtures were stirred for 1 h and then subjected to HPLC analysis (see Supporting Information for the $Sc_3N@C_{80}$ results). As summarized in Figure 14, the Bingel−Hirsch chemical reactivity of $Gd_3N@C_{80}$ in the presence of DMF when directly compared with $Gd_2@C_{79}N$ indicates higher reactivity of $Gd_3N@C_{80}$ with a higher overall yield of mono and significant multiadduct formation (Figure 14a). This reaction was previously reported for $Gd_3N@C_{80}$ in the absence of DMF.[14] In contrast, a lower yield of the $Gd_2@C_{79}N$ monoadduct was obtained after DMF was added to the reaction mixture (Figure 14c). The monoadduct was isolated and characterized by mass spectrometry. Assuming the diethyl bromomalonate anion is the actual intermediate for attack at the carbon sites on the heterofullerene carbon surface, the DFT positive charge

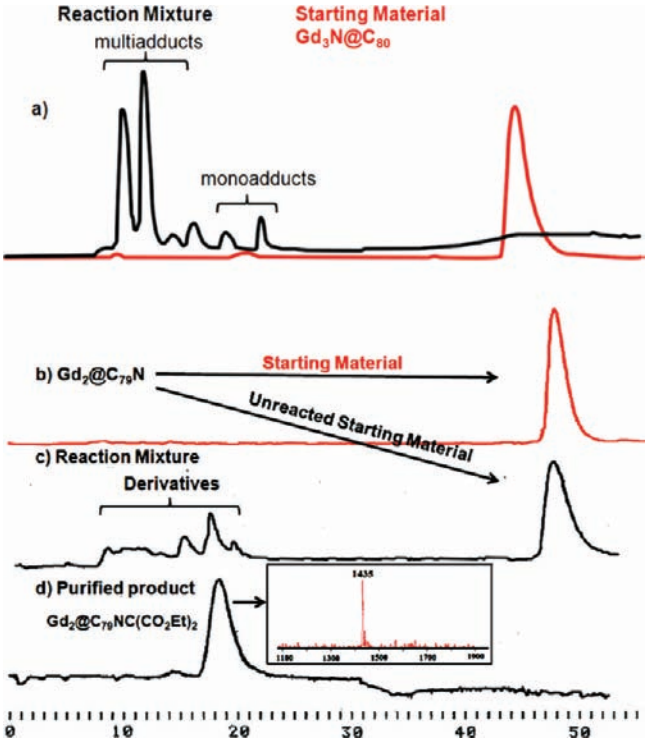

Figure 14. (a) Chromatogram of the Bingel−Hirsch reaction of $Gd_3N@C_{80}$ (a) and $Gd_2@C_{79}N$ (c) with diethyl bromomalonate (10 × 250 mm 5PYE column; λ = 390 nm; flow rate 2.0 mL/min; toluene as eluent; 25 °C) (d) Purified $Gd_2@C_{79}NC(CO_2Et)_2$ monoadduct, laser desorption time-of-flight mass spectrum of the isolated monoadduct.

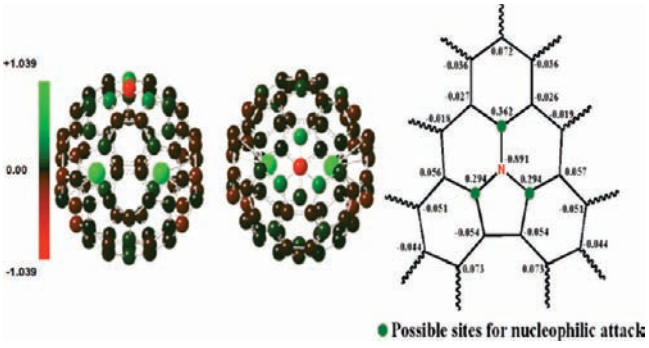

Figure 15. DFT MO charge densities for $Gd_2@C_{79}N$ view from vertical C_2 axis (left), from orthogonal C_2 axis (middle), and carbon surface motif about the N atom (right).

density (green) sites adjacent to the nitrogen atom are likely sites, as illustrated in Figure 15.

The HPLC chromatograms also show that $Gd_3N@C_{80}$ was completely consumed, while about 73% $Sc_3N@C_{80}$ and 83% $Gd_2@C_{79}N$ was retained based on respective peak areas. This suggests $Gd_3N@C_{80}$ has much higher reactivity toward this Bingel reaction than $Sc_3N@C_{80}$ and $Gd_2@C_{79}N$, which reacts in a similar fashion, but limited extent. The reason for the observation is that $Gd_2@C_{79}N$ is less reactive than $Gd_3N@C_{80}$ despite a somewhat lower computed HOMO−LUMO band gap and an electrochemically-derived band gap *vide supra* is not completely understood, but this observation is consistent with previously reported reactivity comparisons between $Gd_3N@C_{80}$, $Gd_3N@C_{84}$ and $Gd_3N@C_{88}$, in which the actual reactivity of the gadofullerenes in the Bingel reaction showed an inverse dependence of predicted stability based on band gap values.[39]

CONCLUSION

In summary, we have prepared, separated and characterized a new dimetallic EHF, $Gd_2@C_{79}N$ in a reasonable yield for the first time. Theoretical and experimental results confirm that this molecule has an unusually high chemical stability and the unpaired electron spin density is centered between the encapsulated Gd_2 cluster. In addition, the spin ($S = {}^1/_2$) on the π orbital of the fullerene cage is coupled with the octet spin ($S = {}^7/_2$) of the encapsulated gadolinium in an antiferromagnetic manner with a small exchange coupling constant. This EPR result suggest the magnetic properties of $Gd_2@C_{79}N$ can be described by a spin quantum number of $S = {}^{15}/_2$ resulting from spin (formally associated with the N atom of the fullerene cage) and two octet spins of the two encapsulated gadolinium ions. Although the heterofullerene $Gd_2@C_{79}N$ is surprisingly unreactive, we have successfully prepared and isolated the first monoadduct of $Gd_2@C_{79}N$. We believe this unique EHF could be very useful in future biomedical, magnetic, and electronic application areas.

ASSOCIATED CONTENT

Supporting Information. Supplementary figures. This material is available free of charge via the Internet at http://pubs.acs.org.

AUTHOR INFORMATION

Corresponding Author

*E-mail: hdorn@vt.edu. Fax: 540-231-3255. Tel: 540-231-5953.

ACKNOWLEDGMENT

We are grateful for support of this work by the National Science Foundation [CHE-0443850 (H.C.D.), DMR-0507083 (H.C.D.)] and the National Institutes of Health [1R01-CA119371-01 (H.C.D.)].

REFERENCES

(1) Prassides, K.; Keshavarz-K, M.; Hummelens, J. C.; Andreoni, W.; Giannozzi, P.; Beer, E.; Bellavia, C.; Cristofolini, L.; Gonzalez, R.; Lappas, A.; Murata, Y.; Malecki, N.; Srdanov, V.; Wudl, F. *Science* **1996**, *271* (5257), 1833–1835.

(2) Poblet, J. M.; Munoz, J.; Winkler, K.; Cancilla, M.; Hayashi, A.; Lebrilla, C. B.; Balch, A. L. *Chem. Commun.* **1999**, *6*, 493–494.

(3) Vostrowsky, O.; Hirsch, A. *Chem. Rev.* **2006**, *106* (12), 5191–5207.

(4) Hummelen, J. C.; Knight, B.; Pavlovich, J.; Gonzalez, R.; Wudl, F. *Science* **1995**, *269* (5230), 1554–1556.

(5) Akasaka, T.; Kato, T.; Kobayashi, K.; Nagase, S.; Yamamoto, K.; Funasaka, H.; Takahashi, T. *Nature* **1995**, *374* (6523), 600–601.

(6) Hou, J. Q.; Kang, H. S. *Chem. Phys.* **2007**, *334* (1−3), 29–35.

(7) Zuo, T.; Xu, L.; Beavers, C. M.; Olmstead, M. M.; Fu, W.; Crawford, D. T.; Balch, A. L.; Dorn, H. C. *J. Am. Chem. Soc.* **2008**, *130* (39), 12992–12997.

(8) Stevenson, S.; Ling, Y.; Coumbe, C. E.; Mackey, M. A.; Confait, B. S.; Phillips, J. P.; Dorn, H. C.; Zhang, Y. *J. Am. Chem. Soc.* **2009**, *131* (49), 17780–17782.

(9) Wilson, L. J.; Cagle, D. W.; Thrash, T. P.; Kennel, S. J.; Mirzadeh, S.; Alford, J. M.; Ehrhardt, G. J. *Coord. Chem. Rev.* **1999**, *190−192*, 199–207.

(10) Bolskar, R. D.; Benedetto, A. F.; Husebo, L. O.; Price, R. E.; Jackson, E. F.; Wallace, S.; Wilson, L. J.; Alford, J. M. *J. Am. Chem. Soc.* **2003**, *125* (18), 5471–5478.
(11) Kato, H.; Kanazawa, Y.; Okumura, M.; Taninaka, A.; Yokawa, T.; Shinohara, H. *J. Am. Chem. Soc.* **2003**, *125* (14), 4391–4397.
(12) Fatouros, P. P.; Corwin, F. D.; Chen, Z.-J.; Broaddus, W. C.; Tatum, J. L.; Kettenmann, B.; Ge, Z.; Gibson, H. W.; Russ, J. L.; Leonard, A. P.; Duchamp, J. C.; Dorn, H. C. *Radiology* **2006**, *240* (3), 756–764.
(13) Sitharaman, B.; Wilson, L. J. *J. Biomed. Nanotechnol.* **2007**, *3* (4), 342–352.
(14) Chaur, M. N.; Melin, F.; Athans, A. J.; Elliott, B.; Walker, K.; Holloway, B. C.; Echegoyen, L. *Chem. Commun.* **2008**, *23*, 2665–2667.
(15) Shu, C.-Y.; Ma, X.-Y.; Zhang, J.; Corwin, F. D.; Sim, J. H.; Zhang, E.-Y.; Dorn, H. C.; Gibson, H. W.; Fatouros, P. P.; Wang, C.-R.; Fang, X.-H. *Bioconjugate Chem.* **2008**, *19* (3), 651–655.
(16) Shu, C.; Corwin, F. D.; Zhang, J.; Chen, Z.; Reid, J. E.; Sun, M.; Xu, W.; Sim, J. H.; Wang, C.; Fatouros, P. P.; Esker, A. R.; Gibson, H. W.; Dorn, H. C. *Bioconjugate Chem.* **2009**, *20* (6), 1186–1193.
(17) Fu, W.; Xu, L.; Azurmendi, H.; Ge, J.; Fuhrer, T.; Zuo, T.; Reid, J. E.; Shu, C.; Harich, K.; Dorn, H. C. *J. Am. Chem. Soc.* **2009**, *131* (33), 11762–11769.
(18) Ge, Z.; Duchamp, J. C.; Cai, T.; Gibson, H. W.; Dorn, H. C. *J. Am. Chem. Soc.* **2005**, *127* (46), 16292–16298.
(19) Frisch, M. J. et al. *GAUSSIAN 09*, Revision A.1; Gaussian, Inc.: Wallingford, CT, 2009.
(20) Adamo, C.; Barone, V. *J. Chem. Phys.* **1999**, *110*, 6158–6170.
(21) Becke, A. D. *J. Chem. Phys.* **1993**, *98*, 5648.
(22) Lee, C.; Yang, W.; Parr, R. G. *Phys. Rev. B* **1988**, *37*, 785.
(23) Stephens, P. J.; Devlin, F. J.; Chabalowski, C. F.; Frisch, M. J. *J. Phys. Chem.* **1994**, *98*, 11623.
(24) Hehre, W. J.; Ditchfield, R.; Pople, J. A. *J. Chem. Phys.* **1972**, *56*, 2257.
(25) Krause, M.; Dunsch, L. *ChemPhysChem* **2004**, *5* (9), 1445–1449.
(26) Elliott, B.; Yu, L.; Echegoyen, L. *J. Am. Chem. Soc.* **2005**, *127* (31), 10885–10888.
(27) Iiduka, Y.; Ikenaga, O.; Sakuraba, A.; Wakahara, T.; Tsuchiya, T.; Maeda, Y.; Nakahodo, T.; Akasaka, T.; Kako, M.; Mizorogi, N.; Nagase, S. *J. Am. Chem. Soc.* **2005**, *127* (28), 9956–9957.
(28) Cai, T.; Xu, L.; Anderson, M. R.; Ge, Z.; Zuo, T.; Wang, X.; Olmstead, M. M.; Balch, A. L.; Gibson, H. W.; Dorn, H. C. *J. Am. Chem. Soc.* **2006**, *128* (26), 8581–8589.
(29) Atsarkin, V. A.; Demidov, V. V.; Vasneva, G. A.; Odintsov, B. M.; Belford, R. L.; Raduechel, B.; Clarkson, R. B. *J. Phys. Chem. A* **2001**, *105* (41), 9323–9327.
(30) Kempinski, W.; Piekara-Sady, L.; Katz, E. A.; Shames, A. I.; Shtutina, S. *Solid State Commun.* **2000**, *114* (3), 173–176.
(31) Furukawa, K.; Okubo, S.; Kato, H.; Shinohara, H.; Kato, T. *J. Phys. Chem.* **2003**, *107* (50), 10933–10937.
(32) Burke, B. G.; Chan, J.; Williams, J. A.; Ge, J.; Shu, C. Y.; Fu, W.; Dorn, H. C.; Kushmerick, J. G.; Puretzky, A. A.; Geohegan, D. B. *Phys. Rev. B: Condens. Matter Mater.* **2010**, *81* (11), 115423/1–115423/7.
(33) Krause, M; Kuzmany, H.; Georgi, P.; Dunsch, L.; Vietze, K.; Seifert, G. *J. Chem. Phys.* **2001**, *115* (14), 6596–6605.
(34) Frisch, M. J. et al. *GAUSSIAN 03*, Revision C.02; Gaussian Inc.: Willingford, CT, 2004.
(35) Burke, B. G.; Chan, T.-W.; Williams, K. A.; Ge, J.; Shu, C. Y.; Fu, W.; Dorn, H. C.; Puretzky, A. A.; Geohegan, D. B. *Mater. Res. Soc. Symp. Proc.* 2009, *1204* (Nanotubes and Related Nanostructures), No. 1204-K10-20.
(36) Nuber, B.; Hirsch, A. *Chem. Commun.* **1998**, *3*, 405–406.
(37) Reszka, K. J.; McCormick, M. L.; Buettner, G. R.; Hart, C. M.; Britigan, B. E. *Nitric Oxide-Biol. Chem.* **2006**, *15* (2), 133–141.
(38) Pinzon, J. R.; Zuo, T.; Echegoyen, L. *Chem.—Eur. J.* 2010, *16* (16), 4864–4869, s4864/1-S4864/15.
(39) Chaur, M. N.; Melin, F.; Elliott, B.; Athans, A. J.; Walker, K.; Holloway, B. C.; Echegoyen, L. *J. Am. Chem. Soc.* **2007**, *129* (47), 14826–14829.
(40) Suzuki, T.; Maruyama, Y.; Kato, T.; Kikuchi, K.; Nakao, Y.; Achiba, Y.; Kobayashi, K.; Nagase, S. *Angew. Chem., Int. Ed.* **1995**, *107*, 1228–1230.